Host–Guest Interaction of 12-MC-4, 15-MC-5, and Fused 12-MC-4 Metallacrowns with Mononuclear and Binuclear Carboxylato Complexes: Structure and Magnetic Behavior

Catherine Dendrinou-Samara,[a] George Psomas,[a] Lykourgos Iordanidis,[b] Vassilis Tangoulis,*[c] and Dimitris P. Kessissoglou*[a]

Abstract: Interaction of manganese with salicylhydroxamic ligands leads to the formation of the 12-membered metallacrown $[Mn^{II}_2(2,4\text{-}DP)_2(HCOO)_2]$-$[12\text{-}MC_{Mn^{III}N(shi)}\text{-}4](py)_6$ (**2**) (H-2,4-DP = 2-(2,4-dichlorophenoxy)propionic acid) and the 15-membered metallacrown $[Mn^{II}(2,4\text{-}D)_2][15\text{-}MC_{Mn^{III}N(shi)}\text{-}5](py)_6$ (**1**) (H-2,4-D = 2,4-dichlorophenoxyacetic acid). The crystal structure analysis shows that mononuclear and dinuclear alkanoato complexes are accommodated in the cavity of the metallacrown ring. The magnetic behaviour of **1** and **2** and the magnetic behaviour of the fused 12-membered metallacrown $[Ni^{II}(mcpa)]_2$-$[12\text{-}MC_{Ni^{II}N(shi)_2(pko)_2}\text{-}4][12\text{-}MC_{Ni^{II}N(shi)_3(pko)}\text{-}4]$-$(CH_3OH)_3(H_2O)$ (**3**) (Hmcpa = 2-methyl-4-chlorophenoxyacetic acid) have shown that the zero field and/or the population of many energy levels at low temperatures is the reason for the divergence of the susceptibility data at high fields. For compound **3**, the ground state is $S = 0$, with $S = 1$ and $S = 2$ low-lying excited states. This leads to a non-Brillouin behaviour of the magnetisation, since the ground state is very close to the excited states.

Keywords: magnetic properties · manganese · metallacrowns · nickel

Introduction

Metallacrowns are a new class of complexes that can be considered to be molecular recognition agents.[1] While many types of molecular species can form complexes, their utility as hosts is quite limited unless there is a mechanism in place to allow the species to distinguish between different guests.[2–6] A number of different approaches can be used to induce changes in a potential host molecule that allow for differentiation of various guests. Among the changes in the host cavity are the size of the cavity, its shape, the number of coordination sites and the type of coordinating species. The correlation between the size of a host cavity and its potential guest is a first criterion for selective molecular recognition. Because of the nature of inorganic molecular recognition agents, it is possible that they could function not only as cation or anion recognition agents, but they may be also able to selectively bind ionic compounds, recognizing the cation and the anion simultaneously.

Metallacrowns have a cyclic structure generally analogous to crown ethers:[7–17] transition metal ions and nitrogen atoms replace the methylene carbons.[18–20] Metallacrown nomenclature is given in Ref. [18]. Previously reported metallacrowns have been prepared from hydroxamic acids and/or ketonximic acids [H_3shi = salicylhydroxamic acid; Hpko = di-(2-pyridyl)-ketonoxime] as constructing ligands. These molecules can act as bifunctional ligands that provide the nitrogen and oxygen donors to the metallacrown ring metals as shown in structure **A** (Scheme 1) for the H_3shi ligand. The triply deprotonated form of shi^{3-}, illustrating the four potential metal

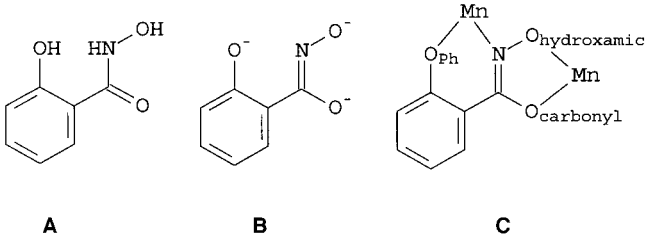

A B C

Scheme 1. The interaction of the salicylhydroxamic acid ligand with metal ions.

[a] Prof. D. P. Kessissoglou, Dr. C. Dendrinou-Samara, Dr. G. Psomas
Department of General and Inorganic Chemistry
Aristotle University of Thessaloniki
Thessaloniki, 54006 (Greece)
Fax: (+30) 31-997-738
E-mail: kessisog@chem.auth.gr

[b] Dr. L. Iordanidis
Department of Chemistry, Michigan State University
East Lansing, MI 48824-1322 (USA)

[c] Dr. V. Tangoulis
Dipartimento di Chimica, Università degli Studi di Firenze
Via Maragliano 75/77, 50144 Florence (Italy)

Supporting information for this article is available on the WWW under http://wiley-vch.de/home/chemistry/ or from the author. Representations of structures **1** and **2** are given as well as their energy spectra as a function of the total spin.

  0947-6539/01/0723-5041 $ 17.50+.50/0

binding sites, is shown as structure **B**. One metal can bind in a five-membered chelate ring formed through the hydroximate group, while a second metal can bind to the six-membered, substituted iminophenolate ring (structure **C**). These juxtaposed five- and six-membered chelate rings form the basis of the metallacrown ring through the (M-N-O-)$_n$ linkage. The cavity size of metallacrowns is similar to that of organic crown ethers. [9-MC$_{M(ox)N(ligand)}$-3],[21–24] [12-MC$_{M(ox)N(ligand)}$-4][25–33] and [15-MC$_{M(ox)N(ligand)}$-5][34–37] metallacrowns, with cavity sizes of 0.35 Å, 0.60 Å and 0.77 Å, respectively, with metal ions Mn^{III}, Fe^{III}, Ni^{II}, Cu^{II} and $V^{V}O$, and stacking metallacrowns[38–40] have already been reported, while the fused $[Ni^{II}(mcpa)]_2$[12-MC$_{Ni^{II}N(shi)_2(pko)_2}$-4][12-MC$_{Ni^{II}N(shi)_3(pko)}$-4]$(CH_3OH)_3(H_2O)$ metallacrown has been described briefly.[41] Cryptates, calixarenes and molecular box motifs in which metal ions replace carbon atoms at the core can also act as inorganic molecular hosts that are capable of selectively binding cationic, anionic and neutral guests.[42–56]

For the 15-MC-5 metallacrowns, two structural motifs have been reported: the planar and the bending motif. Planar 15-MC-5 is formed with Cu^{II} as the ring metal and lanthanides encapsulated in the ring.[22] For the bending motif only one example has been reported so far with Mn^{III} as the ring metal and Mn^{II} as the encapsulated atom.[34] The factors which force the structure into a planar or bending motif are still unknown. Pecoraro at al.[37] claim that a planar analogue of 15-MC-5 could not be accessed with the shi ligand because of the spatial restrictions imposed by having five- and six-membered chelate rings connected. They prepared planar 15-MC-5 by the use of ligands with two adjacent five-membered chelates and an encapsulated metal with a high-coordination number. Both Cu^{II} and Mn^{III} ions show Jahn–Teller distortion but different oxidation states. Our interest is focused on the ability of 15-MC-5 bending metallacrowns to retain their motif on replacement of the encapsulated atom and the accommodated ligands.

For 12-MC-4 compounds, similarities to metal complexes of porphyrins or phthalocyanines with regards to the structural characteristics, cavity size and bite distance apart of 12-C-4 crown ethers, give a new perspective of these compounds as host molecules.[57–61] Taking into account that capping moieties play an important role in the catalytic behaviour of porphyrin or phthalocyanine derivatives towards small molecules, such as O_2 and CO, the exploitation of the nuclearity of the guest molecule of metallacrowns is considered to be an important factor. For 12-MC-4 only mononuclear compounds have been encapsulated to date.

The metallacrowns as a class show quite interesting magnetic behaviour owing to the incorporation of several transition metal ions in close proximity.[1] The structural features of each metallacrown can lead to high magnetic moments per compound through ferromagnetic exchange or coupling to low-lying paramagnetic states. Therefore, we have great interest in the magnetic behaviour of the compounds reported here as they contain two unique structural features: a dinuclear guest molecule accommodated by a 12-MC-4 and a fused 12-MC-4 dimer with high metal nuclearity. Furthermore, until now, there has been no explicit magnetic discussion of polynuclear metallacrowns (>5 magnetic centers) because of the computational difficulties in the calculation of the energy matrix (high dimensions). This, along with the low symmetry that characterises most of them, makes the magnetic analysis a difficult task.

In this paper we report the synthesis, characterisation, the crystal structure and the magnetic behaviour of the 15-membered metallacrown $[Mn^{II}(2,4\text{-}D)_2]$[15-MC$_{Mn^{III}N(shi)}$-5](py)$_6$ (**1**) (H-2,4-D = 2,4-dichlorophenoxyacetic acid) and the 12-membered metallacrown $[Mn^{II}_2(2,4\text{-}DP)_2(HCOO)_2]$-[12-MC$_{Mn^{III}N(shi)}$-4](py)$_6$ (**2**) (H-2,4-DP = 2-(2,4-dichlorophenoxy)propionic acid) and the magnetic behaviour of the fused 12-membered metallacrown $[Ni^{II}(mcpa)]_2$-[12-MC$_{Ni^{II}N(shi)_2(pko)_2}$-4][12-MC$_{Ni^{II}N(shi)_3(pko)}$-4]$(CH_3OH)_3(H_2O)$ (**3**) (Hmcpa = 2-methyl-4-chlorophenoxyacetic acid). Compound **2** is a particularly interesting molecule since it is the first example of a metallacrown with a dinuclear capping complex.

Experimental Section

Materials: The chemicals for the synthesis of the compounds were used as purchased. Dimethylformamide (dmf) was distilled from calcium hydride (CaH_2) and CH_3OH from magnesium (Mg); they were stored over 3 Å molecular sieves. H-2,4-D, H-2,4-DP, H-MCPA, H_3shi, Hpko, $NiCl_2\cdot 6H_2O$ and $MnCl_2\cdot 4H_2O$ were purchased from Aldrich. All chemicals and solvents were reagent grade.

Synthesis of $[Mn^{II}(2,4\text{-}D)_2]$[15-MC$_{Mn^{III}N(shi)}$-5](py)$_6\cdot$py$\cdot$MeOH (1)

Procedure 1: $MnCl_2\cdot 4H_2O$ (0.594 g, 3 mmol) was dissolved in freshly distilled methanol (30 mL). To this was added H_3shi (0.383 g, 2.5 mmol) and CH_3ONa (0.405 g, 7.5 mmol) dissolved in a small amount ($\approx$20 mL) of methanol. The mixture was stirred for 1 h until the colour of the solution became black-brown. An excess of the sodium salt of H-2,4-D (3 mmol) in methanol was added followed by pyridine/methanol (1:10, 100 mL). The black-brown crystalline complex was obtained by slow evaporation of the mother liquid over a period of a few days. Yield 50%.

Procedure 2: $MnCl_2\cdot 4H_2O$ (0.4955 g, 2.5 mmol) was dissolved in methanol (50 mL) and the sodium salt of salicylhydroxamic acid (0.548 g, 2.5 mmol) was added. The mixture was stirred for 1 h until the colour of the solution became black-brown. Pyridine/methanol (1:10, 100 mL) was added followed by excess $[Mn^{II}(2,4\text{-}D)_2(H_2O)_2]_n$ (3 mmol)[67] in methanol. Black-brown crystals of complex **1** that were suitable for X-ray diffraction studies were obtained by slow evaporation of the mother liquid over a period of a few days. Yield: 60%; IR (KBr pellet): $\tilde{\nu}_{max}$ = 1597 (vs) ($C{=}N)_{shi}$, 1568 (s) (asym-$(CO_2)_{2,4\text{-}D}$), 1475 (s) (($C{=}O_{ph})_{shi}$), 1466 (s) (($C{=}O_{ox})_{shi}$), 1440 (s) (sym-$(CO_2)_{2,4\text{-}D}$), 1258 cm^{-1} (s) (($N{-}O_{ox})_{shi}$); UV/Vis (MeOH): λ (ε, dm^{3}mol^{-1}cm^{-1}) = 460 (2217), 345 nm (18614); elemental analysis calcd (%) for $C_{87}H_{69}Cl_4Mn_6N_{12}O_{22}$ (2105.98): C 49.57, H 3.27, N 7.97, Mn 16.67; found: C 49.50, H 3.35, N 7.75, Mn 15.95.

Synthesis of $[Mn^{II}_2(2,4\text{-}DP)_2(HCOO)_2]$[12-MC$_{Mn^{III}N(shi)}$-4](py)$_6\cdot$MeOH (2): $MnCl_2\cdot 4H_2O$(1.2 g, 6 mmol) was dissolved in methanol (50 mL) and a solution of H_3shi (0.6 g, 4 mmol) and MeONa (0.65 g, 12 mmol) in methanol (20 mL) was added dropwise. The reaction mixture was stirred for 1 h until the colour of the solution became dark green-brown. The sodium salt of H-2,4-DP (6 mmol, 1.55 g) was added. After 30 min, a solution of the sodium salt of formic acid (0.41 g, 6 mmol) in pyridine/methanol (1:10, 30 mL) was added. Dark green-brown crystals of complex **2** that were suitable for X-ray diffraction studies were obtained by slow evaporation of the mother liquid over a period of 48 h. Yield 60%; IR (KBr pellet): $\tilde{\nu}_{max}$ = 1595 (vs) ($C{=}N)_{shi}$), 1567 (s) (asym-$(CO_2)_{2,4\text{-}DP}$), 1515 (s) (asym-$(CO_2)_{formato}$), 1479 (s) (($C{=}O_{ph})_{shi}$), 1464 (s) (($C{=}O_{ox})_{shi}$), 1433 (s) (sym-$(CO_2)_{2,4\text{-}DP}$), 1392 (s) (sym$(CO_2)_{formato}$), 1255 cm^{-1} (s) (($N{-}O_{ox})_{shi}$); UV/Vis (DMF): λ (ε) = 640 (812), 450 (sh) (8200), 365 nm (20830); elemental analysis calcd (%) for $C_{79}H_{66}Cl_4Mn_6N_{10}O_{23}$ (1994.78): C 47.52, H 3.31, N 7.02, Mn 16.54; found: C 47.40, H 3.40, N 6.80, Mn 16.20.

$[Ni^{II}(mcpa)]_2$[12-MC$_{Ni^{II}N(shi)_2(pko)_2}$-4][12-MC$_{Ni^{II}N(shi)_3(pko)}$-4]$(CH_3OH)_3(H_2O)$ (3): The synthesis of compound **3** has already been reported.[41]

0947-6539/01/0723-5042 $ 17.50+.50/0 *Chem. Eur. J.* **2001**, *7*, No. 23

Physical measurements: IR spectra ($\nu = 200-4000\ cm^{-1}$) were recorded on a Perkin–Elmer FT-IR 1650 spectrometer with samples prepared as KBr pellets. UV/VIS spectra were recorded on a Shimadzu-160A dual-beam spectrophotometer. C, H and N elemental analysis were performed on a Perkin–Elmer 240B elemental analyser; Mn and Ni were determined by atomic absorption spectroscopy on a Perkin–Elmer 1100B spectrophotometer. Electric conductance measurements were carried out with a WTW model LF530 conductivity setup and a type C cell, which had a cell constant of 0.996. This represents a mean value calibrated at 25 °C with potassium chloride. Polycrystalline powder EPR spectra were recorded for all the compounds at X-band frequency (9.23 GHz) on a Varian ESR 9 spectrometer equipped with a continuous-flow 4He cryostat both at room temperature and at helium temperatures from 4 K to 30 K . The temperature dependence of the magnetic susceptibility was measured on polycrystalline powder samples with a Cryogenics S600 SQUID magnetometer with an applied field of 0.1–1.0 T and in temperature range 2–300 K. Data were corrected with the standard procedure for the contribution of the sample holder and diamagnetism of the sample.

X-ray crystal structure determination: A black-brown crystal of **1** with dimensions of $0.36 \times 0.14 \times 0.06\ mm^3$ and a dark green-brown crystal of **2** with dimensions of $0.40 \times 0.18 \times 0.13\ mm^3$ were mounted on the top of glass fibres. Data were collected at $-100.1(1)$ °C and -120 °C respectively, with a Bruker (formerly Siemens) SMART Platform CCD diffractometer equipped with an Oxford Cryosystems "Cryostream" low-temperature system. Crystal data and parameters for data collection of **1** and **2** are presented in Table 1.

For **1**, a little over a hemisphere of data (1639 frames) was collected. Final cell constants were calculated from a set of 4517 strong reflections [$I > 10\sigma(I)$] obtained from the data collection. For **2**, almost a full sphere of data (1949 frames) was collected. Final cell constants were calculated from a set of 13889 strong reflections [$I > 10\sigma(I)$] obtained from the data collection. Four different sets of frames were collected with 0.30° steps in ω. The exposure time per frame was 35 s for **1** and 40 s for **2** and the detector-to-crystal distance was ≈ 5 cm. The resolution of the data set was 0.78 Å and 0.71 Å, respectively. The SMART[62] software was used for data acquisition and SAINT[63] for data extraction. The absorption correction was carried out with SADABS[64] and all refinements with the SHELXTL[65] and/or SHELX 97[66] package of crystallographic programs. The structures were solved by direct methods. All the non-hydrogen atoms were refined anisotropically. The hydrogen atoms were placed in idealised positions and refined with a riding model. The largest shift/esd on the final cycle was 0.000.

For **2** the structure consists of molecules of genral formula $[Mn_6(shi)_4(2,4\text{-}DP)_2(HCOO)_2(py)_6]$. Three crystallographically independent methanol molecules were located in the empty space between the Mn molecules. The occupancy of the methanol molecules was refined; however, because their refinement was unstable, their occupancies and isotropic temperature factors were constrained and not refined. The largest shift/esd on the final cycle was 0.023.

Crystallographic data (excluding structure factors) for the structures reported in this paper have been deposited with the Cambridge Crystallographic Data Centre as supplementary publication no. CCDC-171892 (**1**) and CCDC-171893 (**2**). Copies of the data can be obtained free of charge on application to CCDC, 12 Union Road, Cambridge CB2 1EZ, UK (fax: (+44) 1223-336-033; e-mail: deposit@ccdc.cam.ac.uk).

Results and Discussion

Synthesis of the complexes: The synthesis of the 15-membered metallacrown **1** was achieved by two methods:

1) The reaction of $MnCl_2 \cdot 4H_2O$ with the deprotonated salicylhydroxamic acid followed by the addition of the sodium salt of the phenoxyalkanoic acid in 10:1 mixture of methanol/pyridine [Eq. (1)]:

$$6\,MnCl_2 \cdot 4H_2O + 5\,Na_3shi + 2\,Na(2,4\text{-}D) \longrightarrow [Mn_6(2,4\text{-}D)_2(shi)_5(py)_6] \text{ or } [Mn^{II}(2,4\text{-}D)_2][15\text{-}MC_{Mn^{III}N(shi)}\text{-}5](py)_6\ (\mathbf{1}) \quad (1)$$

2) The reaction of $MnCl_2 \cdot 4H_2O$ with the deprotonated salicylhydroxamic acid in a 10:1 mixture of methanol/pyridine followed by the addition of an excess of the manganese complex of the phenoxyalkanoic acid [Eq. (2)]:

$$5\,MnCl_2 \cdot 4H_2O + 5\,Na_3shi + [Mn(2,4\text{-}D)_2(H_2O)_2]_n \longrightarrow [Mn_6(2,4\text{-}D)_2(shi)_5(py)_6] \text{ or } [Mn^{II}(2,4\text{-}D)_2][15\text{-}MC_{Mn^{III}N(shi)}\text{-}5](py)_6\ (\mathbf{1}) \quad (2)$$

The compound is black-brown crystalline solid, soluble in methanol and pyridine, and is not an electrolyte in methanol.

The synthesis of the 12-membered metallacrown was achieved by the reaction of $MnCl_2 \cdot 4H_2O$, H_3shi and MeONa in methanol, followed by the addition of the sodium salts of H2,4-DP and formic acid in 10:1 mixture of methanol/pyridine [Eq. (3)]:

$$6\,MnCl_2 \cdot 4H_2O + 4\,H_3shi + 12\,CH_3ONa + 2\,Na(2,4\text{-}DP) + 2\,HCOONa \longrightarrow Mn_6(2,4\text{-}D)_2(HCOO)_2(shi)_4(py)_6] \text{ or } [Mn^{II}{}_2(2,4\text{-}DP)_2(HCOO)_2][12\text{-}MC_{Mn^{III}N(shi)}\text{-}4](py)_6\ (\mathbf{2}) \quad (3)$$

The compound is a dark green-brown crystalline solid, soluble in methanol and pyridine, and is not an electrolyte in methanol.

Structure of complex 1: The ORTEP diagram of the metallacrown core and the hosted manganese carboxylato complexes of the crystal structure of complex **1** is given in Figure 1, while the whole metallacrown ring is more understandable as Scheme 2. Crystallographic data are given in Table 1 and important bond lengths and angles are given in Table 2. The metallacrown was prepared from salicylhydroxamic acid (H_3shi). The ligand acts as a bifunctional ligand and provides the nitrogen and oxygen as donors to the Mn^{III} in the metallacrown ring. One Mn^{III} binds in a five-membered chelate ring formed through the hydroximate group, while a second Mn^{III} binds to the six-membered, substituted iminophenolate ring. These juxtaposed five- and six-membered chelate rings form the basis of the metallacrown ring through the $(Mn\text{-}N\text{-}O\text{-})_n$ linkage. The crystal structure contains a neutral 15-membered metallacrown ring of the type [15-$MC_{Mn^{III}N(shi)}$-5] formed by five structural moieties of the type (Mn^{III}-N-O) (Scheme 2). The $(Mn\text{-}N\text{-}O)_5$ connectivity is emphasized by bold bonds in Figure 1. The specific connectivity of atoms to form the ring is: Mn1-O1-N1-Mn2-O7-N3-Mn4-O13-N5-Mn3-O10-N4-Mn5-O4-N2. The average Mn^{III}–Mn^{III} separation in the metallacrown ring is 4.642 Å, the bite distance is 2.744 Å and the cavity size is 0.77 Å. This provides sufficient space for the encapsulation of Mn^{II} (ionic radius 0.83 Å).

Four sites of the coordination sphere of the ring Mn^{III} ions are filled by the heteroatoms of two shi ligands. The remaining sites are filled with nitrogen or oxygen atoms of the pyridine and the carboxylato groups, respectively.

A diversity in the geometry of the five Mn^{III} has been observed: three Mn atoms, Mn2, Mn3 and Mn4, adopt a propeller-like structure with three long ($Mn-(O/N)_{av} = 2.181$ Å) and three short bond lengths ($Mn-(O/N)_{av} = 1.915$ Å) and have Λ, Λ and Δ stereochemistry, respectively.

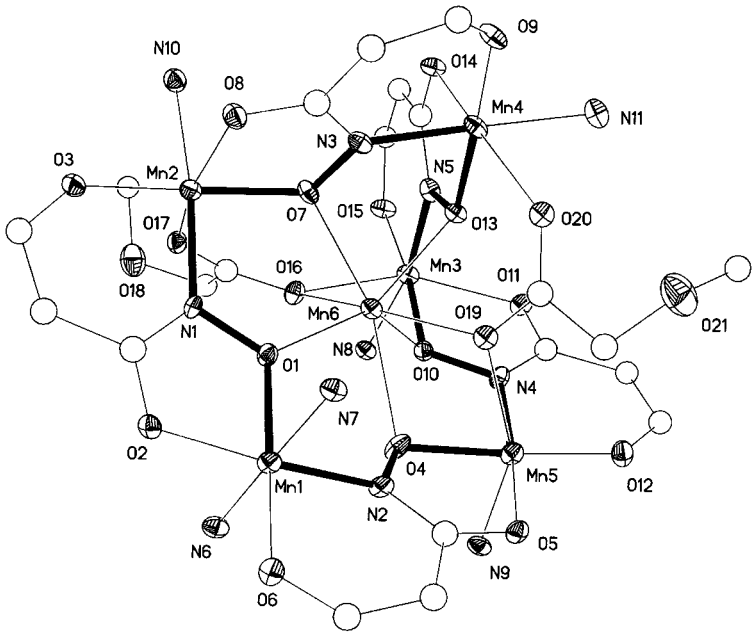

Figure 1. An ORTEP diagram of $[Mn^{II}(2,4\text{-}D)_2][15\text{-}MC_{Mn^{III}N(shi)}\text{-}5](py)_6 \cdot py \cdot MeOH$ (**1**) with 25% ellipsoids of the heteroatoms and with only the heteroatoms labelled; the metallacrown core, the coordination environment of the ring Mn^{III} ions and the coordination mode of the encapsulated Mn^{II} atom are highlighted.

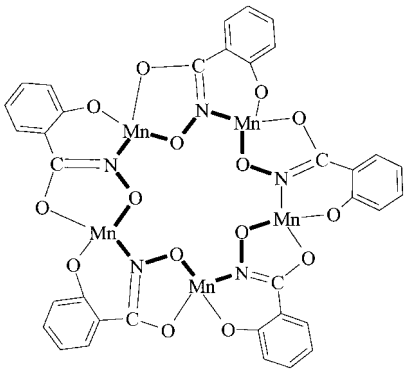

Scheme 2. The manganese 15-MC-5 metallacrown ring.

The remaining two Mn^{III} atoms, Mn1 and Mn5, are planar with four short $(Mn-(O/N)_{av} = 1.913$ Å) and two long $(Mn-(O/N)_{av} = 2.368$ Å) bond lengths (Scheme 3).

The diversity in the configuration (planar or propeller) for the ring Mn^{III} ions gives flexibility to the metallacrown core and simultaneously allows the encapsulation of the sixth Mn^{II}, Mn6. The encapsulated metal ion is manganese(II), since there are five shi^{3-} ligands, five Mn^{III} ions in the crown and two carboxylato ligands. The encapsulated Mn^{II} is seven-coordinate and is bound to the five hydroximato oxygen donors (O1, O4, O7, O10 and O13) provided by the metallacrown core, as well as to two oxygen atoms from the carboxylate herbicide ligands 2,4-D (O16 and O19 or O20′). The Mn^{II} to Mn^{III} separations are, on average, 3.481 Å. The average Mn^{II} to ring Mn^{III} separation of 12-MC-4 is 3.54 Å.

The two alkanoato ligands result in a further stabilisation of the complex and are bound on opposite faces of the 15-MC-5 (Figure 1). The carboxylato group of the 2,4-D ligand is bound to manganese atoms in triple bidentate mode (bifurcated). The first carboxylate group is bound through O16 to the encapsulated Mn6 and ring Mn3 to form a monoatomic oxygen bridge(Mn3–O16 = 2.438(5) Å, Mn6–O16 = 2.267(4) Å), while O17 is bound to ring Mn2 (Mn2–O17 = 2.239(5) Å). The second carboxylato group contains two disordered oxygen atoms, O19/O19′ and O20/O20′. The occupancy factors are 0.84 for O19 and O20 and 0.16 for O19′ and O20′. O19 is bound to the encapsulated Mn6 and ring Mn5 atoms, while O20 is bound to the ring Mn4 atom. The disordered O19′ is bound to the ring Mn5 atom and O20′ to the central Mn6 and ring Mn4 atoms.

Table 1. Crystal data and structure refinement[a] for compounds **1** and **2**.

	1	**2**
formula	$C_{87}H_{69}Cl_4Mn_6N_{12}O_{22}$	$C_{79.14}H_{66.56}Cl_4Mn_6N_{10}O_{23.14}$
M_r	2105.98	1999.34
T [K]	173(2)	173(2)
λ [Å]	0.71073	0.71073
crystal system	triclinic	orthorhombic
space group	$P\bar{1}$	$Pna2_1$
a [Å]	12.5438(9)	26.060(3)
b [Å]	16.169(1)	22.294(2)
c [Å]	23.793(1)	14.6659(14)
α [°]	70.259(1)	90
β [°]	78.187(1)	90
γ [°]	76.225(2)	90
V [Å^3]	4370.4(5)	8520.5(14)
Z	2	4
ρ_{calcd} [Mg m^{-3}]	1.600	1.559
μ [mm^{-1}]	1.045	1.067
$F(000)$	2138	4058
θ range [°]	1.39–27.15	2.40–29.87
index ranges	$-16 \le h \le 15$	$-35 \le h \le 35$
	$-20 \le k \le 18$	$-29 \le k \le 29$
	$-30 \le l \le 30$	$-20 \le l \le 18$
reflections collected/unique	32982/18631 [R(int) = 0.0885]	85549/22134 [R(int) = 0.0938]
completeness to θ	27.15 96.3%	29.87 94.8%
data/restraints/parameters	18631/0/736	22134/1/1084
goodness-of-fit on F^2	0.931	0.937
final R indices [$I > 2\sigma(I)$]	$R1 = 0.0798$, $wR2 = 0.1651$	$R1 = 0.0585$, $wR2 = 0.1322$
R indices(all data)	$R1 = 0.2212$, $wR2 = 0.2012$	$R1 = 0.1419$, $wR2 = 0.1587$
largest diff. peak/hole [e Å^{-3}]	0.824/−0.949	1.283/−0.731
absolute structure parameter	–	0.008(16)
extinction coefficient	–	0.00010(10)

[a] Refinement method for both complexes: full-matrix least-squares on F^2.

0947-6539/01/0723-5044 $ 17.50+.50/0 *Chem. Eur. J.* **2001**, *7*, No. 23

Table 2. Selected bond lengths [Å] of compound **1**.

planar Mn^{III}			
$Mn1-O6_{phenolate}$	1.855(5)	$Mn5-O12_{phenolate}$	1.857(5)
$Mn1-O1_{hydroximate}$	1.921(5)	$Mn5-N4_{hydroximate}$	1.920(6)
$Mn1-O2_{carbonyl}$	1.935(5)	$Mn5-O5_{carbonyl}$	1.928(4)
$Mn1-N2_{hydroximate}$	1.944(6)	$Mn5-O4_{hydroximate}$	1.943(5)
$Mn1-N6_{pyridine}$	2.339(6)	$Mn5-N9_{pyridine}$	2.295(6)
$Mn1-N7_{pyridine}$	2.389(5)	$Mn5-O19'_{2,4-D}$	2.42(3)
		$Mn5-O19_{2,4-D}$	2.4826
propeller Mn^{III}			
Mn^{III} stereochemistry, Λ		Mn^{III} stereochemistry, Λ	
$Mn2-O3_{phenolate}$	1.852(5)	$Mn3-O15_{phenolate}$	1.829(5)
$Mn2-O7_{hydroximate}$	1.895(5)	$Mn3-O10_{hydroximate}$	1.918(4)
$Mn2-N1_{hydroximate}$	2.017(6)	$Mn3-N5_{hydroximate}$	1.968(6)
$Mn2-O8_{carbonyl}$	2.124(5)	$Mn3-N8_{pyridine}$	2.115(5)
$Mn2-N10_{pyridine}$	2.128(6)	$Mn3-O11_{carbonyl}$	2.147(5)
$Mn2-O17_{2,4-D}$	2.239(5)	$Mn3-O16_{2,4-D}$	2.438(5)
Mn^{III} stereochemistry, Δ		Encapsulated Mn^{II}	
$Mn4-O9_{phenolate}$	1.828(5)	$Mn6-O10_{hydroximate}$	2.207(5)
$Mn4-O13_{hydroximate}$	1.918(4)	$Mn6-O1_{hydroximate}$	2.230(5)
$Mn4-N3_{hydroximate}$	2.010(6)	$Mn6-O7_{hydroximate}$	2.231(5)
$Mn4-N11_{pyridine}$	2.107(6)	$Mn6-O19_{2,4-D}$	2.241(6)
$Mn4-O14_{carbonyl}$	2.131(4)	$Mn6-O13_{hydroximate}$	2.244(4)
$Mn4-O20_{2,4-D}$	2.198(6)	$Mn6-O16_{2,4-D}$	2.267(4)
$Mn4-O20'_{2,4-D}$	2.41(3)	$Mn6-O4_{hydroximate}$	2.342(5)
		$Mn6-O20'_{2,4-D}$	2.4503

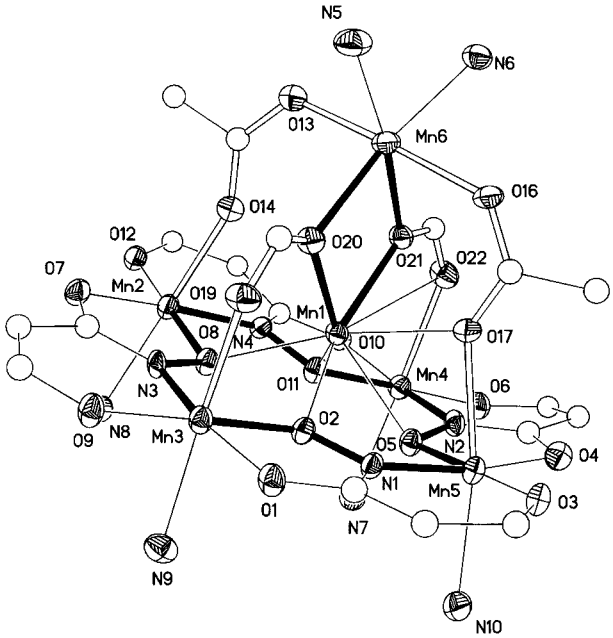

Figure 2. An ORTEP diagram of $[Mn^{II}_2(2,4\text{-DP})_2(HCOO)_2]$-$[12\text{-}MC_{Mn^{III}N(shi)}\text{-}4](py)_6 \cdot 1.14\,MeOH$ (**2**) with 25% ellipsoids with only the heteroatoms labelled; the metallacrown core, the coordination environment of the ring Mn^{III} ions and the coordination mode of the hosted binuclear Mn^{II} complex are emphasized.

Structure of complex 2: The ORTEP diagram of the crystal structure of complex **2** is given in Figure 2. Important bond lengths and angles are given in Table 3 . The X-ray structure of **2** consists of a neutral 12-membered metallacrown of the type $[12\text{-}MC_{Mn^{III}N(shi)}\text{-}4]$. Four ring Mn^{III} atoms and four salicylhydroximato (shi^{3-}) ligands construct the formally neutral $[12\text{-}MC_{Mn^{III}N(shi)}\text{-}4]$ core. The shi^{3-} ligands act as a binucleating tetradentate ligand and binds one ring Mn^{III} atom through the iminophenolato N and O_{Ph} in a six-membered chelate ring and a second ring Mn^{III} atom through the carbonyl and hydroxamato oxygens (O_C and O_H) in a juxtaposed five-membered chelate. The juxtaposed five- and six-membered chelates form the basis of the metallacrown structure through a (Mn^{III}-N-O) ring system. The specific connectivity of the atoms to form the ring is: Mn2-O8-N3-Mn3-O2-N1-Mn5-O5-N2-Mn4-O11-N4.

All of the Mn^{III} ions participating in the metallacrown are six-coordinate in a planar configuration with pyridine nitrogens and carboxylato oxygens bound in the apical positions of a Jahn–Teller elongated octahedron. The average separation between manganese atoms in the ring, $Mn^{III}\cdots Mn^{III}$, of 4.628 Å and the bite distance of 2.744 Å are very similar to those reported for $[Mn(acetate)_2][12\text{-}MC_{Mn^{III}N(shi)}\text{-}4](dmf)_6$, (4.64 Å and 2.73 Å, respectively), which is a 12-membered metallacrown with a mononuclear $[Mn(acetate)_2]$ complex in the capping position.[26] The cavity size of 0.645 Å is similar to analogous organic 12-crown-4 (0.60 Å) and a little larger than the analogous $[Mn(acetate)_2][12\text{-}MC_{Mn^{III}N(shi)}\text{-}4](dmf)_6$, (0.57 Å).

The 12-membered manganese(III) metallacrown hosts the binuclear complex $[Mn^{II}_2(2,4\text{-DP})_2(HCOO)_2(py)_2]$ as a capping molecule. It contains a Mn_2O_2 core with the two oxygen atoms provided by the two formato ligands, each contributes a carboxylato oxygen as a bridging atom between the two Mn^{II} ions. With regards to the coordination of the two Mn^{II} ions, Mn1 is seven-coordinate and Mn6 is six-coordinate. The Mn1 coordination environment is completed by the four metal-

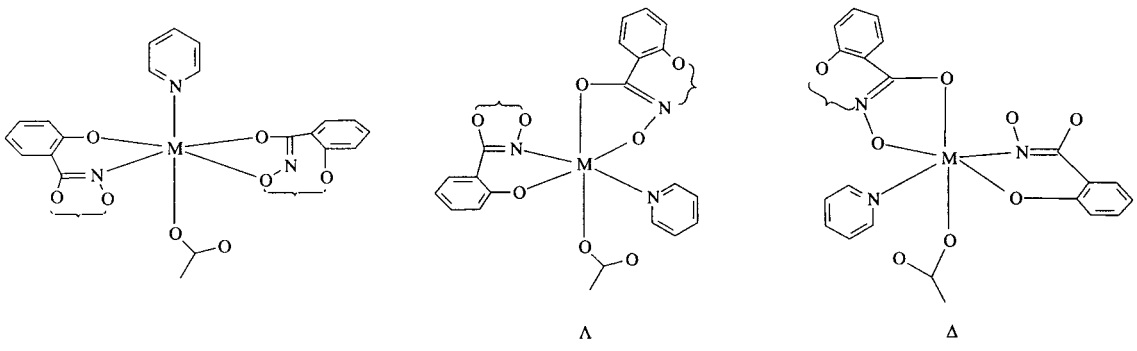

Scheme 3. The planar and propeller configurations for the Mn^{III} ring ions.

Table 3. Selected bond lengths [Å] and angles [°] for compound **2**.

ring Mn^{III}			
$Mn2-O12_{phenolate}$	1.861(4)	$Mn3-O9_{phenolate}$	1.860(4)
$Mn2-O8_{hydroximate}$	1.893(4)	$Mn3-O2_{hydroximate}$	1.889(4)
$Mn2-O7_{carbonyl}$	1.959(4)	$Mn3-O1_{carbonyl}$	1.994(4)
$Mn2-N4_{hydroximate}$	1.956(4)	$Mn3-N3_{hydroximate}$	1.971(5)
$Mn2-O14_{2,4-D}$	2.185(4)	$Mn3-O19_{formate}$	2.205(4)
$Mn2-N8_{pyridine}$	2.319(5)	$Mn3-N9_{pyridine}$	2.340(6)
$Mn4-O6_{phenolate}$	1.845(4)	$Mn5-O3_{phenolate}$	1.846(4)
$Mn4-O8_{hydroximate}$	1.898(4)	$Mn5-O2_{hydroximate}$	1.889(4)
$Mn4-O10_{carbonyl}$	1.944(5)	$Mn5-O1_{carbonyl}$	1.994(4)
$Mn4-N2_{hydroximate}$	1.944(5)	$Mn5-N3_{hydroximate}$	1.961(4)
$Mn4-O22_{formate}$	2.267(4)	$Mn5-O19_{formate}$	2.205(4)
$Mn4-N7_{pyridine}$	2.317(5)	$Mn5-N9_{pyridine}$	2.340(6)
encapsulated Mn^{II} (Mn1)		encapsulated Mn^{II} (Mn6)	
$Mn1-O2_{hydroximate}$	2.229(4)	$Mn6-O20_{formate}$	2.231(4)
$Mn1-O5_{hydroximate}$	2.305(4)	$Mn6-O21_{formate}$	2.201(4)
$Mn1-O8_{hydroximate}$	2.269(4)	$Mn6-N5_{pyridine}$	2.237(6)
$Mn1-O20_{formate}$	2.202(4)	$Mn6-O16_{2,4-D}$	2.142(4)
$Mn1-O11_{hydroximate}$	2.237(4)	$Mn6-N6_{pyridine}$	2.290(5)
$Mn1-O21_{formate}$	2.199(3)	$Mn6-O13_{2,4-D}$	2.146(5)
$Mn1-O17_{2,4-D}$	2.457(4)		
O21-Mn1-O20	81.26(14)	Mn1-O20-Mn6	98.48(15)
O21-Mn6-O20	80.57(14)	Mn1-O21-Mn6	99.48(15)

lacrown ring oxygens (O2, O5, O8 and O11), by O20 and O21 from the two bridging formato ligands and by O17 of a 2,4-D terminal ligand. Mn6 is bound to the alkanoato oxygens, O13 and O16, as well as to the two bridging formato oxygens O20 and O21, while the remaining sites for the Mn6 octahedron are filled by nitrogen atoms (N5 and N6) of two pyridine molecules.

The dinuclear Mn_2O_2 core is almost planar (the sum of the angles O21-Mn1-O20 = 81.26(14)°, O21-Mn6-O20 = 80.57(14)°, Mn1-O20-Mn6 = 98.48(15)° and Mn1-O21-Mn6 = 99.48(15)° is 359.79° and the torsion angle O21-Mn1-O20-Mn6-O20 = 3.4°) with the two manganese(II) ions, Mn1 and Mn6, displaced out of the best least-squares plane defined by O2, O5, O8 and O11 by 1.295 Å and 4.644 Å, respectively. The Mn1 ··· Mn6 separation is 3.358 Å and falls into the range for triply-bridged Mn^{II} ions,[67] for example, 3.35 Å in $[Mn(C_2H_5COO)_2(H_2O)_2]$,[68] and 3.289 Å in $[Mn_3(CH_3COO)_2(bpc)_2(py)_4(H_2O)_2]$, ($H_2bpc$ = 2,2′-bipyridyl-3,3′-dicarboxylic acid),[69] while it is smaller than 3.53 Å reported for the analogous double-bridged monodentate doubly-bound coordination mode of carboxylato ligands of $[Mn_2(C_6H_2Cl_3\text{-}OCH_2COO)_4](H_2O)_4]$.[70]

The two formato ligands are in triple bidentate coordination mode and bridge through O20 and O21, respectively, the inward encapsulated manganese atom Mn1 and the outward capped manganese atom Mn6, while each formato group also bridges through oxygen atoms O19 and O20 or O21 and O22 the encapsulated Mn1 with the ring manganese Mn4 and manganese Mn3, respectively (empty bonds in Figure 2). The separations between Mn1 and Mn6 to the ring Mn^{III} are, on average, 3.471 Å and 5.574 Å, respectively.

The two 2,4-DP carboxylato ligands show a diverse coordination mode. One ligand is bound in bidentate *syn–anti* bridging fashion to Mn6 and to the ring manganese atoms Mn2, while the second one is coordinated in a triple bidentate mode bridging in *syn–anti* fashion the Mn6 and the ring manganese atom Mn5, while O17 is bound also to Mn1. Both 2,4-DP ligands are *cis* with respect to the metallacrown ring. These bridges enclose the encapsulated trigonal-prismatic Mn6 ion through two almost equally long paths of Mn6-O13-C29-O14-Mn2 (= 6.85 Å) and Mn6-O16-C38-O17-Mn5 (= 6.90 Å) (empty bonds in Figure 2).

Structure of complex 3: The X-ray structure of **3** has already been reported.[41] Here we give a general description of the structure that is necessary for the understanding of the magnetic interaction.

The X-ray structure[41] of **3** consists of two [12-$MC_{M(ox)N(ligand)}$-4] units: $[Ni^{II}(mcpa)][12\text{-}MC_{Ni^{II}N(shi)_2(pko)_2}\text{-}4](CH_3OH)_2$ and $[Ni^{II}(MCPA)][12\text{-}MC_{Ni^{II}N(shi)_3(pko)}\text{-}4](CH_3OH)(H_2O)$ with charges of +1 and −1, respectively. Each unit has four Ni^{II} ring ions and one additional encapsulated Ni^{II} ion. The five Ni^{II} atoms of each metallacrown core are in the same plane with an angle between these two planes of 3.8°. The central nickel geometry is octahedral with an average distance from the ring to the central atom of 3.31 Å and 3.33 Å in the anion and cation, respectively. The anionic unit is bound to cationic unit to create binuclear moieties (Ni1-O71-Ni2-O21), (Ni3-O1-Ni6-O73), (Ni5-O61-Ni7-O23) and (Ni9-N11-Ni10-O22) with Ni1 ··· Ni2 = 3.142 Å, Ni1 ··· Ni10 = 3.594 Å, Ni2 ··· Ni4 = 3.671 Å, Ni3 ··· Ni6 = 3.230 Å and Ni5 ··· Ni7 = 3.071 Å in a planar arrangement. The $[Ni^{II}(mcpa)][12\text{-}MC_{Ni^{II}N(shi)_2(pko)_2}\text{-}4](CH_3OH)_2$ cation, has an alternating pattern of shi^{3-} and pko^- ligands around the 12-MC-4 structure to form a neutral metallacrown ring. All Ni^{II} have an octahedral configuration, except Ni8 which has a square-planar configuration. The $[Ni^{II}(mcpa)][12\text{-}MC_{Ni^{II}N(shi)_3(pko)}\text{-}4](CH_3OH)(H_2O)$ anion with three shi^{3-} and one pko^- ligands forms an anionic metallacrown ring moiety with a charge of −2 and with an overall anion charge of −1. The configuration around the Ni^{II} atoms is analogous to that in the cationic metallacrown with Ni4 now in a square-planar environment (Figure 3).

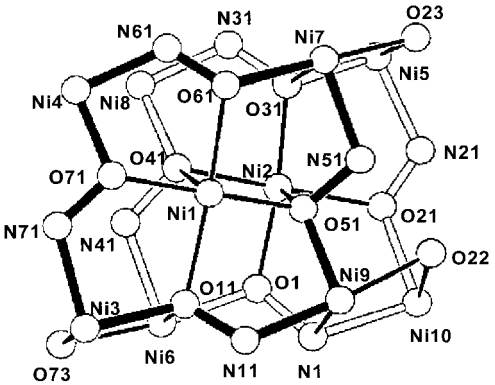

Figure 3. A view of $[Ni^{II}(MCPA)]_2[12\text{-}MC_{Ni^{II}N(shi)_2(pko)_2}\text{-}4][12\text{-}MC_{Ni^{II}N(shi)_3(pko)}\text{-}4](CH_3OH)_3(H_2O)$ (**3**) showing the interaction between the two metallacrowns.

Magnetic study of 3: The temperature dependence of the susceptibility data of **3**, in the form of $\chi_M T$, is shown in Figure 4a. The susceptibility decreases from a value of 8.2 $cm^3 mol^{-1} K$ at 300 K to 2.19 $cm^3 mol^{-1} K$ at 2 K. The value at room temperature is smaller than that of 9.68 $cm^3 mol^{-1} K$

0947-6539/01/0723-5046 $ 17.50+.50/0 *Chem. Eur. J.* **2001**, *7*, No. 23

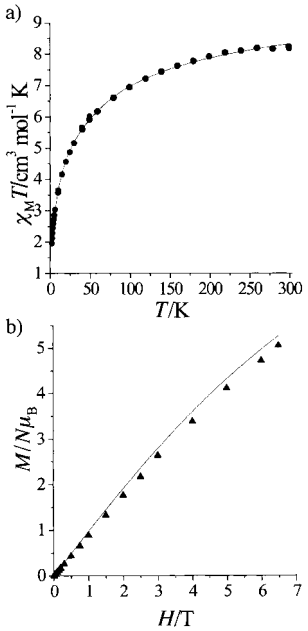

Figure 4. a) Temperature dependence of the susceptibility data, in the form of $\chi_M T$ of **3** at 0.1 T. The solid line represents the best fit according to Equation (4). Inset: the low-temperature dependence of the susceptibility at 0.1 T and 1 T. See text for details. b) Magnetisation measurements, in the reduced form of $M/N\mu_B$ versus HT^{-1} [TK^{-1}] in the field range 0–6.5 T at 2 K and 4.6 K of complex **3**.

expected for eight independent ions with $S=1$, that has a g value equal to 2.2. This reveals the overall antiferromagnetic character of the system. From crystallographic criteria, the exchange pathways in this complex are both ferromagnetic and antiferromagnetic and the magnetic interpretation of it becomes very difficult owing to 1) the large number of different exchange couplings and 2) the size of the energy matrix which in the present case is 6561×6561, considering that two Ni atoms (Ni4 and Ni8) are diamagnetic. In order to overcome this problem, different magnetic models (2-*J*, 3-*J*, 4-*J*) were used to examine the important exchange pathways and the possible correlation between the exchange parameters. To confirm the validity of the values obtained from the fitting procedure, simulations of the magnetisation curve were carried out with the values obtained from the susceptibility data. With regards to the second problem, the successive use of the ITO (irreducible tensor operator) techniques[71, 72] was employed; this allowed us to take full account of all kinds of magnetic exchange interactions as well as to exploit the symmetry associated with the total spin functions in such a way that the exchange matrix initially of size 6561×6561, is formed by *S*-block matrices with a maximum size of 280×280. In this treatment the spin anisotropy of nickel(II) has been neglected to take full advantage of the spin symmetry, otherwise the problem becomes almost intractable for our computational capabilities. Because of the complex nature of the coupling scheme in this cluster and the following ones, a more graphical way of representation will be used. According to this representation, the magnetic centres are presented along with, from the magnetic point of view, the most important bridging pathways. All other bridging modes are omitted for clarity. Thus, the magnetic model that was used is shown graphically in Scheme 4; only the oxo-bridges are taken into consideration for more effective coupling and the exchange pathways linking nickel atoms for distances less

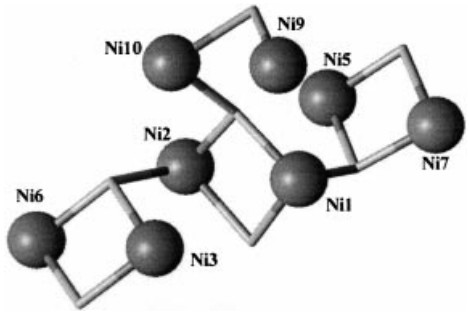

Scheme 4. The magnetic model used for **3** with the oxo-bridges and the exchange pathways linking nickel atoms at distances <3.3 Å.

than 3.3 Å. With this treatment the zero-field hamiltonian given in Equation (4) was used:

$$H = J_1(S_1S_7 + S_2S_{10}) + J_2(S_1S_2) + J_3(S_3S_6) + J_4(S_5S_7) + J_5(S_9S_{10}) \quad (4)$$

It must be pointed out that even with these assumptions, the hamiltonian formalism was not simplified because of the differences in the various exchange pathways. By fixing the value of g to 2.2, the following J values were obtained: $J_1 = 68.8$ cm^{-1}, $J_2 = 98.35$ cm^{-1}, $J_3 = 5.19$ cm^{-1}, $J_4 = -1.65$ cm^{-1} and $J_5 = -48.43$ cm^{-1}. There values are in agreement with magnetostructural correlations found in other nickel(II) clusters.[73, 74] The theoretical curve is shown in the Figure 4a as a solid line. Table 4 gives selected bonds lengths and angles

Table 4. Structural characteristics of the model in Scheme 4.

J values	Bond lengths [(Å]		Bond angles [°]	
J_3	Ni3–Ni6	3.229	Ni3-O73-Ni6	101.1(1)
			Ni3-O1-Ni6	98.69(1)
J_2	Ni2–Ni1	3.143	Ni2-O21-Ni1	101.1(1)
			Ni2-O71-Ni1	93.46(1)
J_1	Ni2–Ni10	3.207	Ni2-O21-Ni10	107.3(5)
	Ni1–Ni7	3.182	Ni1-O61-Ni7	103.5(1)
J_4	Ni5–Ni7	3.078	Ni5-O23-Ni7	95.54(1)
			Ni5-O61-Ni7	97.40(1)
J_5	Ni9–Ni10	3.059	Ni9-O22-Ni10	90.51(1)

according to Scheme 4. According to the data, the large antiferromagnetic values of J_1 and J_2 are in agreement with the general magnetostructural correlation, namely, for Ni-O-Ni angles $>100^\circ$ the interaction is antiferromagnetic and the reason for $J_1 < J_2$ is possibly the single oxo character the bridge between Ni1 and Ni7 and between Ni2 and Ni10 compared to the most effective double oxo bridge between Ni2 and Ni1. The small J_3 exchange interaction is in agreement with the larger distance between Ni3 and Ni6 and the smaller Ni-O-Ni angle (compared to the previous pairs). It is quite important to note here that the model predicts the large ferromagnetic interaction between the Ni9 and Ni10, which has the smallest distance (3.058 Å) and the smallest Ni-O-Ni angle (90.5°). The case of the J_4 interaction is also interesting:

here the values of the Ni-O-Ni angles are close to the ferro/antiferro limit and the value of J_4 is small although the Ni – Ni distance is almost the same as the previous ferromagnetic pair. Evidently, the reasonable over-parameterisation of the model may involve possible correlations between the J values. In order to test this set of parameters, the theoretical magnetisation curve obtained from them was compared to the experimental curve in Figure 4b. The model reproduces the linear dependence of the magnetisation with the field moderately well. The magnetisation curve was measured at 4.7 K in order to avoid spin anisotropy[75] of the cluster at lower temperatures; at this temperature the splitting of the lower spin levels caused by the anisotropy is smaller than the thermal energy and, therefore, all these levels are populated. To completely model a magnetic system it would be necessary to measure the entire "magnetisation surface", the three-dimensional space defined by temperature, external magnetic field and the resulting magnetisation. Usually we have only two sections in this space, namely, variable-temperature susceptibility at one fixed field and variable-field magnetisation at one fixed temperature. As a consequence, the best-fit parameters for the former *may not agree* with those of the latter.

The reason for this linearity in the magnetisation curve is clearly resolved by examining the energy spectrum of the complex (see the Supporting Information). The ground state of the system is $S=0$ with an $S=1$ at 0.6 cm^{-1} and an $S=2$ at 1.7 cm^{-1} above $S=0$, respectively. This leads to non-Brillouin behaviour of the magnetisation because the ground state is very close to the excited states.[75]

Magnetic study of 1: The temperature dependence of the susceptibility data of **1**, in the form of $\chi_M T$, is shown in Figure 5a. The susceptibility decreases from a value of 17.2 $cm^3 mol^{-1} K$ at 300 K to 1.4 $cm^3 mol^{-1} K$ at 2.2 K. The value at room temperature is smaller than the value of 19.375 $cm^3 mol^{-1} K$ (for five independent ions with $S=2$ and one $S=5/2$ when $g=2$). This reveals the overall antiferromagnetic character of the system. While the number of exchange pathways in this system is smaller compared to the previous complex, the size of the exchange matrix has increased considerably to 18750×18750. The successive use of ITO techniques reduces the size to S-block matrices with a maximum size of 330×330. The magnetic model that was used is shown in Scheme 5; only the oxo bridges have been taken into consideration for more effective coupling and the exchange interactions are defined mainly according to the Mn-O-Mn angle and the distance between the Mn ions. Exchange interactions for distances of >4 Å were excluded. The corresponding zero-field hamiltonian formalism is given in Equation (5).

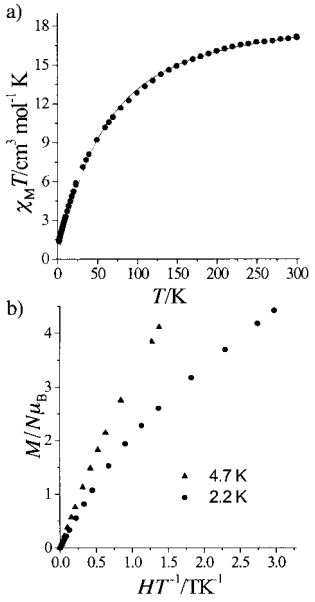

Figure 5. a) Temperature dependence of the susceptibility data, in the form of $\chi_M T$ of **1** at 0.1 T. The solid line represents the best fit according to Equation (5). See text for details. b) Magnetisation measurement, in the reduced form of $M/N\mu_B$, in the field range 0 – 6.5 T at 5 K of complex **1**. The solid line represents the simulation according to the values obtained from the fit of the susceptibility data.

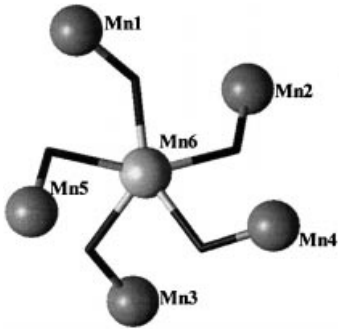

Scheme 5. The magnetic model used for **1** showing the oxo-bridges and the exchange interactions between the Mn ions.

$$H = J_1 S_6(S_3 + S_5) + J_2 S_6(S_1 + S_2) + J_3(S_6 S_4) \quad (5)$$

The results of the fitting are: $J_1 = -9.0\ cm^{-1}$, $J_2 = J_3 = 14.6\ cm^{-1}$ (which was confirmed with a 2-J model as well), $g=2.0$. The theoretical curve is shown in Figure 5a as a solid line. Although there are no exact magnetostructural correlations between the Mn^{III}-O-Mn^{II} angle and the sign/magnitude of the exchange constant, it has been shown that for Mn^{III}-O-Mn^{II} angles of $\approx 120^\circ$ the interaction is antiferromagnetic,[76–80] while for $\approx 105^\circ$ the interaction is still ferromagnetic.[81] According to the data given in Table 5, the above considerations are in agreement with the fitted results. The fit was valid for the data from 30 K to 300 K, but fails to explain the low-temperature behaviour of the system. A possible reason for this low-temperature behaviour maybe the large zero-field splitting and/or the intermolecular interactions.[76] In order to further test the validity of the ferromagnetic interaction (J_1)

Table 5. Structural characteristics of the model in Scheme 5.

J values	Bond lengths [(Å]		Bond angles [°]	
J_2	Mn6–Mn2	3.579	Mn6-O1-Mn1	123.9(1)
	Mn6–Mn1	3.666	Mn6-O7-Mn2	120.09(1)
J_1	Mn6–Mn5	3.368	Mn6-O4-Mn5	103.2(1)
	Mn6–Mn3	3.317	Mn6-O10-Mn3	106.84(1)
J_3	Mn6–Mn4	3.476	Mn6-O13-Mn4	112.9(1)

0947-6539/01/0723-5048 $ 17.50+.50/0 *Chem. Eur. J.* **2001**, *7*, No. 23

predicted by the model between the Mn6 and Mn3, Mn5, theoretical curves were calculated by fixing the J_2 value and replacing J_1 by the values $+1$, $+100$, -1, $-100\ cm^{-1}$ for the small/large antiferro/ferromagnetic interaction, respectively. It can be seen in Figure 6, that when the interaction between

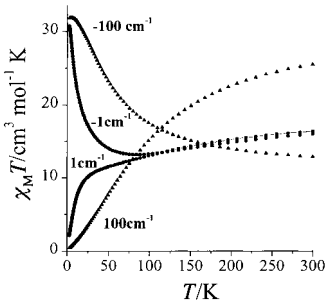

Figure 6. Simulations of the susceptibility according to Equation (5) by variation of the J_1 value and fixing the J_2 value according to the results obtained for the fitting of the susceptibility data of complex **1**. See text for details.

the Mn6 and the Mn3, Mn5 is antiferromagnetic (small or large) a high ground state, $S = 15/2$, is stabilised which in agreement with a spin-up configuration for $S_1 = 5/2$, $S_5 = S_1 = 2$ with all the others spins down or opposite. Then the susceptibility gradually decreases to smaller values. In this case, in which the interaction is ferromagnetic, the susceptibility data at low temperatures is close to 0 and gradually increases to higher values. This discrepancy between the theoretical and the experimental susceptibility at low temperatures was further investigated with magnetisation measurements at different temperatures. The results are shown in Figure 5b for two temperatures (2.2 and 4.7 K). The data are plotted in the form of reduced magnetisation, $M/N\mu_B$, as a function of the magnetic field divided by the corresponding temperature. The reason for doing this is to discover the magnitude of the difference in the magnetisation behaviour at different temperatures, bearing in mind that magnetisation data at different temperatures can be superimposed if they have Brillouin behaviour.[82] It seems that the difference is quite large starting from low magnetic fields and this is proof for the existence of large zero-field and/or intermolecular interactions in the low-temperature limit. Furthermore, the population of many energy states at these temperatures is also a possibility for this behaviour of the magnetisation data. In this treatment, the spin anisotropy has been neglected to take full advantage of the spin symmetry, otherwise the problem also becomes intractable.

Magnetic study of 2: The temperature dependence of the susceptibility data of **2**, in the form of $\chi_M T$, is shown in Figure 7a. It decreases from a value of 19.44 $cm^3 mol^{-1} K$ at 300 K to 7.36 $cm^3 mol^{-1} K$ at 2 K. The value at room temperature is smaller than the value of 20.75 $cm^3 mol^{-1} K$ expected for four independent ions with $S = 2$ and two $S = 5/2$, when $g = 2$. This reveals the overall antiferromagnetic character of the system. The size of the exchange matrix increased even more considerably and was $22\,500 \times 22\,500$. The successive use of ITO techniques reduces the size to *S*-block matrices with a

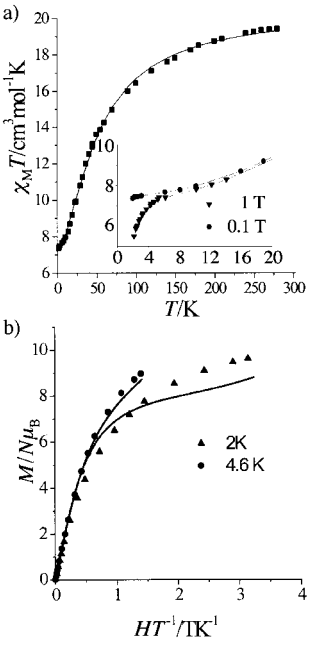

Figure 7. a) Temperature dependence of the susceptibility data, in the form of $\chi_M T$ of **2** at 0.1 T. The solid line represents the best fit according to Equation (6). See text for details. b) Magnetisation measurements, in the reduced form of $M/N\mu_B$ versus HT^{-1} [TK^{-1}] in the field range 0–6.5 T at 2.2 K and 4.7 K of complex **2**.

maximum size of 365×365. The magnetic model that was used is shown in Scheme 6; the same considerations as for the previous complex were taken into account in order to build the corresponding hamiltonian formalism [Eq. (6)]:

$$H = J_1(S_1S_5) + J_2S_1(S_2 + S_3 + S_4) + J_3(S_1S_6) \quad (6)$$

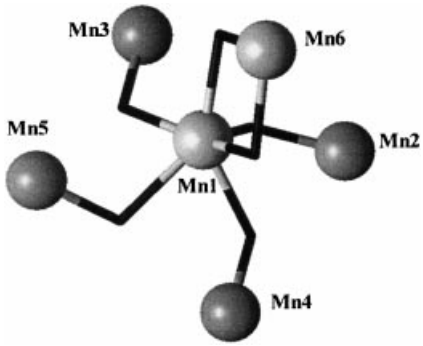

Scheme 6. The magnetic model used for **2** showing the oxo-bridges and the exchange interactions between the Mn ions.

The results of the fitting are: $J_1 = -9.5\ cm^{-1}$, $J_2 = 8.3\ cm^{-1}$, $J_3 = 0.17\ cm^{-1}$, $g = 2.0$. The theoretical curve is also shown Figure 7a as a solid line. Table 6 gives selected bond lengths and angles according to Scheme 6. It is important to note that in this complex the ferromagnetic interaction (J_1) and the antiferromagnetic interaction (J_2) also have the same nature as in the previous complex and is a direct proof of the validity of the fit, while the small antiferromagnetic interaction (J_3) is in agreement with the known magnetostructural correlations.

Table 6. Structural characteristics of the model in Scheme 6.

J values	Bond lengths [Å]		Bond angles [°]	
J_1	Mn1–Mn5	3.374	Mn1-O5-Mn5	106.7(1)
J_2	Mn1–Mn2	3.458	Mn1-O8-Mn2	112.06(1)
	Mn1–Mn4	3.517	Mn1-O11-Mn4	116.3(1)
	Mn1–Mn3	3.533	Mn1-O2-Mn3	117.95(1)
J_3	Mn6–Mn1	3.358	Mn6-O21-Mn1	99.49(1)
			Mn6-O20-Mn1	98.48(1)

Furthermore, in the inset of Figure 7a the low-temperature magnetic data are shown for two different magnetic fields, 0.1 and 1 T, respectively. In order to explore the nature of this divergence at high fields (saturation effects or zero-field effects) magnetisation measurements were carried out at different temperatures and are shown in Figure 7b for two temperatures 2.0 and 4.6 K. By the use of the same method to plot the magnetisation data as in the previous case, it is evident that the zero-field and/or the population of many energy levels at low temperatures is the reason for this divergence of the susceptibility data at high fields. A simulation of the magnetisation data was then carried out with the set of parameters obtained from the treatment of the susceptibility data and the results are also shown in Figure 7b as solid lines. The simulation is in very good agreement at high temperatures (4.6 K), while at 2 K it diverges significantly. This divergence is attributed to the fact that we did not take into account the zero-field splitting effects which are more important at this temperature.[75] According to the energy spectrum of the complex, the ground state is $S = 4$ with an $S =$ 3, 2, 1 at $\approx$0.5, 1.0, 1.5 cm^{-1} above the ground state, respectively; this again leads to this non-Brillouin behaviour of the magnetisation (the Supporting Information)

Finally, X-band powder EPR measurements were carried out in the temperature range 4–60 K: there is a single resonance which is centered at $g = 2$. In the inset of Figure 8,

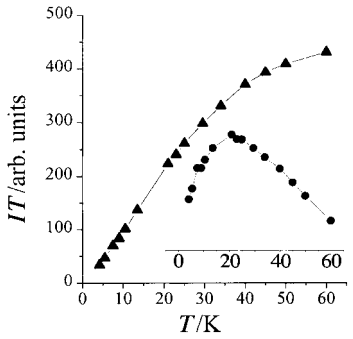

Figure 8. Temperature dependence of the intensity of the powder X-band EPR resonance of **2**, centered at $g = 2.0$, in the form of IT, and in the temperature range 4–60 K. Inset: the temperature dependence of the intensity is shown; there is a clear peak at $\approx$23 K.

the temperature dependence of the intensity of this resonance is shown. There is a maximum at $\approx$23 K. The product of the intensity with the temperature is also shown. The dependence of this product does not follow the Curie law; this is a direct proof that the resonance belongs to a cluster with many populated states near its ground state.

Conclusion

While 12-MC-4 and 15-MC-5 metallacrowns have been reported previously, some very interesting features are presented in this report. Compound **2** is the first example of a structurally characterised 12-MC-4 compound that has a dinuclear encapsulated complex which permits the use of a larger variety of guest molecules. We have shown that the zero-field and/or the population of many energy levels at low temperatures is the reason for the divergence of the susceptibility data at high fields. For the first time, in the case of compound **3**, an attempt was made to fit the magnetic data of a compound of high nuclearity ($10\,Ni^{II}$). The ground state is $S = 0$ with $S = 1$ and $S = 2$ low-lying excited states. This leads to non-Brillouin behaviour of the magnetisation because the ground state is very close to the excited states.

Acknowledgement

The authors thank Dr. Sanakis for his assistance with the EPR experiments. This work was supported in part by the 3MD EU Network (Contract No.: ERB 4061 PL 97–0197).

[1] V. L. Pecoraro, A. J. Stemmler, B. R. Gibney, J. J. Bodwin, H. Wang, J. W. Kampf, A. Barwinski, *Prog. Inorg. Chem.* **1997**, *45*, 83.
[2] G. M. Gray, *Comments Inorg. Chem.* **1995**, *17*, 95.
[3] E. C. Constable, *Prog. Inorg. Chem.* **1994**, *41*, 67.
[4] C. J. Pederson, *Angew. Chem.* **1988**, *100*, 1053; *Angew. Chem. Int. Ed. Engl.* **1988**, *27*, 1021.
[5] D. J. Cram, G. M. Lein, *J. Am. Chem. Soc.* **1985**, *107*, 3657.
[6] D. J. Cram, *Angew. Chem.* **1988**, *100*, 1041; *Angew. Chem. Int. Ed. Engl.* **1988**, *27*, 1009.
[7] J.-M. Lehn, *Acc. Chem. Res.* **1978**, *11*, 49.
[8] C. J. Pederson, *J. Am. Chem. Soc.* **1967**, *89*, 2495.
[9] C. J. Pederson, *J. Am. Chem. Soc.* **1967**, *89*, 391.
[10] C. J. Pederson, *J. Am. Chem. Soc.* **1970**, *92*, 386.
[11] C. J. Pederson, H. K. Frensdorf, *Angew. Chem.* **1972**, *84*, 16; *Angew. Chem. Int. Ed. Engl.* **1972**, *11*, 1.
[12] C. J. Pedersen, in *Synthetic Multidentate Macrocyclic Compounds* (Eds.: R. M. Izatt, J. J. Christensen), Academic Press, New York, **1978**, p. 1.
[13] C. J. Pedersen, *J. Am. Chem. Soc.* **1967**, *89*, 2495.
[14] E. Weber, J. L. Toner, I. Goldberg, F. Vogtle, D. A. Stoddart, R. A. Bartsch, C. L. Liotta, *Crown Ethers and Analogs*, Wiley, New York, **1989**, 558.
[15] M. Hiraoka, *Crown Ethers Analogous Compd.* **1992**, *45*, 485.
[16] P. Dastidar, Z. Stein, I. Goldberg, C. E. Stouse, *Supramol. Chem.* **1996**, *7*, 257.
[17] Y.-H. Kiang, G. B. Gardner, S. Lee, E. B. Lobkovsky, *J. Am. Chem. Soc.* **1999**, *121*, 8204.
[18] Metallacrown nomenclature: The nomenclature used for metallacrowns is as follows: $M'_mA_a[X\text{-}MC_{M^{n+}H(Z)}\text{-}Y]$, where X and Y indicate the ring size and number of oxygen donor atoms, respectively, MC specifies a metallacrown, M and $n+$ are the ring metal and its oxidation state, H is the identity of the remaining heteroatom bridge, and (Z) is an abbreviation for the organic ligand containing the N/O functionality. There are m captured metals (M′) and a bridging anions (A) bound to the ring oxygens and metals, respectively. Thus, a metal-encapsulated metallacrown is represented by $[Mn(2,4\text{-}DP)_2][15\text{-}MC_{Mn^{III}N(shi)5}\text{-}5]$. This molecule has the core structure of 15-crown-5 with the carbon atoms replaced by Mn^{III} and N atoms throughout the ring. The trianion of salicylhydroxamic acid (shi^{3-}) confers stability to the ring.[19, 20] A single Mn^{II} is captured by the hydroxamate oxygens, and there are two bridging carboxylato ligands linking two ring metals

  0947-6539/01/0723-5050 $ 17.50+.50/0

to the captured metal. A full treatment of additional descriptors of chirality for the ring and captured metal ions is given in ref. [1].
[19] A. Bagno, C. Couzzi, G. Scorrano, *J. Am. Chem. Soc.* **1994**, *116*, 916.
[20] O. N. Ventura, J. B. Rama, L. Turi, J. J. Danenberg, *J. Am. Chem. Soc.* **1993**, *115*, 5754.
[21] M. S. Lah, V. L. Pecoraro, *Comments Inorg. Chem.* **1990**, *11*, 59.
[22] G. Psomas, A. J. Stemmler, C. Dendrinou-Samara, J. J. Bodwin, M. Schneider, M. Alexiou, J. Kampf, D. P. Kessissoglou, V. L. Pecoraro, *Inorg. Chem.* **2001**, *40*, 1562.
[23] V. L. Pecoraro, *Inorg. Chim. Acta* **1989**, *155*, 171.
[24] M. S. Lah, M. L. Kirk, W. Hatfield, V. L. Pecoraro, *J. Chem. Soc. Chem. Commun.* **1989**, 1606.
[25] B. R. Gibney, A. J. Stemmler, S. Pilotek, J. W. Kampf, V. L. Pecoraro, *Inorg. Chem.* **1993**, *32*, 6008.
[26] M. S. Lah, V. L. Pecoraro, *J. Am. Chem. Soc.* **1989**, *111*, 7258.
[27] M. S. Lah, V. L. Pecoraro, *Inorg. Chem.* **1991**, *30*, 878.
[28] B. Kurzak, E. Farkas, T. Glowiak, H. Kozlowski, *J. Chem. Soc. Dalton Trans.* **1991**, 163.
[29] B. R. Gibney, J. W. Kampf, D. P. Kessissoglou, V. L. Pecoraro, *Inorg. Chem.* **1994**, *33*, 4840.
[30] A. J. Stemmler, J. W. Kampf, V. L. Pecoraro, *Inorg. Chem.* **1995**, *34*, 2271.
[31] A. J. Stemmler, J. W. Kampf, M. L. Kirk, V. L. Pecoraro, *J. Am. Chem. Soc.* **1995**, *117*, 6368.
[32] D. P. Kessissoglou, J. J. Bodwin, J. Kampf, C. Dendrinou-Samara, V. L. Pecoraro, *Inorg. Chim. Acta*, in press.
[33] Y. Song, J-C. Liu, D-R. Zhu, J-Z. Zhuang, X-Z. You, *Inorg. Chim. Acta* **2000**, *305*, 135.
[34] D. P. Kessissoglou, J. W. Kampf, V. L. Pecoraro, *Polyhedron* **1994**, *13*, 1379.
[35] A. J. Stemmler, J. W. Kampf, V. L. Pecoraro, *Angew. Chem.* **1996**, *108*, 3005; *Angew. Chem. Int. Ed. Engl.* **1996**, *35*, 2841.
[36] A. D. Cutland, R. G. Malkani, J. W. Kampf, V. L. Pecoraro, *Angew. Chem.* **2000**, *112*, 2801; *Angew. Chem. Int. Ed. Engl.* **2000**, *39*, 2689.
[37] A. J. Stemmler, J. W. Kampf, M. L. Kirk, B. H. Atasi, V. L. Pecoraro, *Inorg. Chem.* **1999**, *38*, 2807.
[38] R. W. Saalfrank, R. Burak, S. Reihs, N. Löw, F. Hampel, H.-D. Stachel, J. Lentmaier, K. Peters, E.-M. Peters, H. G. von Schering, *Angew. Chem.* **1995**, *107*, 1115; *Angew. Chem. Int. Ed. Engl.* **1995**, *34*, 993.
[39] R. W. Saalfrank, I. Bernt, E. Uller, F. Hampel, *Angew. Chem.* **1997**, *109*, 2596; *Angew. Chem. Int. Ed. Engl.* **1997**, *36*, 2482.
[40] R. W. Saalfrank, N. Löw, S. Kareth, V. Seitz, F. Hampel, D. Stalke, M. Teichert, *Angew. Chem.* **1998**, *110*, 182; *Angew. Chem. Int. Ed.* **1998**, *37*, 172.
[41] G. Psomas, C. Dendrinou-Samara, M. Alexiou, A. Tsohos, C. P. Raptopoulou, A.Terzis, D. P. Kessissoglou, *Inorg. Chem.* **1998**, *37*, 6556.
[42] G. W. Gokel, *J. Chem. Soc. Rev.* **1992**, 39.
[43] J.-M. Lehn, J. P. Sauvage, *J. Am. Chem. Soc.* **1975**, *97*, 6700.
[44] J.-M. Lehn, *Acc. Chem. Res.* **1978**, *11*, 49.
[45] J.-M. Lehn, F. Montavon, *Helv. Chim. Acta* **1978**, *61*, 67.
[46] J.-M. Lehn, *Science* **1985**, *219*, 1177.
[47] M. S. Lah, B. R. Gibney, D. L. Tierney, J. E. Penner-Hahn, V. L. Pecoraro, *J. Am. Chem. Soc.* **1993**, *115*, 5857.
[48] A. J. Blake, R. O. Gould, C. M. Grant, P. E. Y. Milne, D. Reed, R. E. P. Winpenny, *Angew. Chem.* **1994**, *106*, 208; *Angew. Chem. Int. Ed. Engl.* **1994**, *33*, 195.
[49] A. J. Blake, R. O. Gould, P. E. Y. Milne, D. Reed, R. E. P. Winpenny, *J. Chem. Soc. Chem. Commun.* **1991**, 1453.
[50] C. D. Gutsche, *Acc. Chem. Res.* **1983**, *16*, 161.
[51] C. D. Gutsche, *Calixarenes: A Versitile Class of Macrocyclic Compounds*, Kluwer Academic, Boston **1991**, p. 3.
[52] H. Ruter, E. C. Hillgeris, A. Erxleben, B. Lippert, *J. Am. Chem. Soc.* **1994**, *116*, 616.
[53] M. Fujita, J. Yazaki, K. Ogura, *J. Am. Chem. Soc.* **1990**, *112*, 5645.
[54] J. Stang, K. Chen, *J. Am. Chem. Soc.* **1995**, *117*, 1667.
[55] P. J. Stang, D. H. Cao, *J. Am. Chem. Soc.* **1994**, *116*, 4981.
[56] P. J. Stang, V. V. Zhdankin, *J. Am. Chem. Soc.* **1993**, *115*, 9808.
[57] J. Arnold, *J. Chem. Soc. Chem. Commun.* **1990**, 976.
[58] J. Arnold, D. Y. Dawson, C. G. Hoffman, *J. Am. Chem. Soc.* **1993**, *115*, 2707.
[59] H. Brand, J. A. Capriotti, *Inorg. Chem.* **1994**, *33*, 4334.
[60] H. Sugimoto, M. Mori, H. Masuda, T. Taga, *J. Chem. Soc. Chem. Commun.* **1986**, 962.
[61] R. F. Ziolo, W. H. H. Günther, J. M. Troup, *J. Am. Chem. Soc.* **1981**, *103*, 4629.
[62] SMART v5.049–5.054, **1998**, Bruker Analytical X-ray Systems, Madison, Wisconsin 53719 (USA).
[63] SAINT v5.0–6.01, **1998**, Bruker Analytical X-ray Systems, Madison, Wisconsin 53719 (USA).
[64] G. M. Sheldrick, SADABS, University of Göttingen (Germany).
[65] SHELXTL v5.1, **1999** Bruker Analytical X-ray Systems, Madison, Wisconsin 53719 (USA).
[66] G. M. Sheldrick, SHELX 97, University of Göttingen (Germany).
[67] V. Tangoulis, G. Psomas, C. Dendrinou-Samara, C. P. Raptopoulou, A. Terzis, D. P. Kessissoglou, *Inorg. Chem.* **1996**, *35*, 7655.
[68] T. Lis, *Acta Crystallogr. Sect. B* **1977**, *33*, 2964.
[69] Z. J. Zhong, X-Z. You, *Polyhedron* **1994**, *13*, 2157.
[70] C. H. L. Kennard, G. Smith, E. J. O'Reilly, W. Chiangjin, *Inorg. Chim. Acta* **1983**, *69*, 53.
[71] D. Gatteschi, L. Pardi, *Gazz. Chim. It.* **1993**, *123*, 231.
[72] D. Gatteschi, A. Caneschi, R. Sessoli, A. Cornia, *Chem. Soc. Rev.* **1996**, 101.
[73] J. M. Clemente-Juan, E. Coronado, J. R. Galán-Mascaros, C. J. Gómez-García, *Inorg. Chem.* **1999**, *38*, 55.
[74] J. M. Clemente-Juan, B. Chansou, B. Donnadieu, J.-P. Tuchagues, *Inorg. Chem.* **2000**, *39*, 5515.
[75] J. J. Borrás-Almenar, J. M. Clemente-Juan, E. Coronado, B. S. Tsukerblat, *Inorg. Chem.* **1999**, *38*, 6081.
[76] D. P. Kessissoglou, M. L. Kirk, M. S. Lah, X.-h. Li, C. A. Raptopoulou, W. E.Hatfield, V. L. Pecoraro, *Inorg. Chem.* **1992**, *31*, 5424.
[77] D. A. Malamatari, P. Hitou, A. G. Hatzidimitriou, F. E. Inscore, A. Gourdon, M. L. Kirk, D. P. Kessissoglou, *Inorg. Chem.* **1995**, *34*, 2493.
[78] V. Tangoulis, D. A. Malamatari, K. Soulti, V. Stergiou, C. P. Raptopoulou, A. Terzis, T. A. Kabanos, D. P. Kessissoglou, *Inorg. Chem.* **1996**, *35*, 4974.
[79] D. P. Kessissoglou, *Coord. Chem. Rev.* **1999**, *185/186*, 837.
[80] V. Tangoulis, D. A. Malamatari, G. A. Spyroulias, C. P. Raptopoulou, A. Terzis, D. P. Kessissoglou, *Inorg. Chem.* **2000**, *39*, 2621.
[81] M. Hirotsu, M. Kojima, Y. Yoshikawa, *Bull. Chem. Soc. Jpn* **1997**, *70*, 649.
[82] C. Delfs, D. Gatteschi, L. Pardi, R. Sessoli, K. Wieghardt, D. Hanke, *Inorg. Chem.* **1993**, *32*, 3099.

Received: February 6, 2001
Revised: July 9, 2001 [F3058]